Rapid Communications

Induced Ising spin-orbit interaction in metallic thin films on monolayer WSe_2

Yingying Wu,* James Jun He,* Tianyi Han, Shuigang Xu, Zefei Wu, Jiangxiazi Lin, Ting Zhang, Yuheng He, and Ning Wang†
Department of Physics and the Center for Quantum Materials, The Hong Kong University of Science and Technology, Hong Kong, China

(Received 5 December 2018; published 11 March 2019)

Spin-orbit interaction (SOI) in superconductors can protect Cooper pairs from external magnetic fields and thus enhance the upper critical field. This effect is most significant in ultrathin superconductor films when the field is in plane. Recently, it was found that this protection is especially efficient in so-called Ising superconductors whose special form of SOI pins the electron spins in the out-of-plane direction and the in-plane critical field is enhanced up to tens of Tesla. We report that a strong SOI can be induced in metallic thin films by proximity to monolayer tungsten diselenide (WSe_2), a semiconductor with intrinsic strong Ising SOI. We demonstrate that the upper critical field of the thin-film superconductor is enhanced by the induced SOI, even though the zero-field critical temperature is unchanged or reduced.

DOI: 10.1103/PhysRevB.99.121406

Two-dimensional (2D) materials other than graphene, such as black phosphorus [1–5], and atomically thin transition-metal dichalcogenides (TMDs) [6–11] have attracted a lot of attention since the wide application of the micromechanical exfoliation technique. TMDs, including MoS_2, $MoSe_2$, WS_2, WSe_2, etc., are van der Waals materials with unique and promising electrical and optical properties [12–14]. When the thickness of TMDs goes from bulk to monolayer, the electronic band gap transforms from an indirect one to a direct one. Strong SOI exhibiting in TMDs, especially in monolayers [15–19], pins the electron spin in the out-of-plane direction. With this kind of intrinsic strong SOI, the superconducting members of TMDs, namely, Ising superconductors [6,20], own a protected superconductivity against the in-plane magnetic field and thus an extremely large in-plane critical field up to tens of Tesla. This is because the paramagnetic effect on the Cooper pairs of the in-plane field becomes small compared to the spin pinning effect of Ising SOI. In conventional superconductors such as aluminum (Al) and niobium (Nb), the orbital effect and Zeeman effect of the magnetic field will quench the superconductivity and make the critical magnetic field usually smaller than the Clogston-Chandrasekhar Pauli limit [21]. Researchers have tried to increase the spin-orbit scattering in these conventional thin-film superconductors by coating submonolayer thickness of Pt in previous studies [22], but the investigation of inducing SOI from layered TMDs to these thin-film superconductors remains elusive. Recent theoretical calculations indicate that the strong SOI in TMDs can be induced into conventional superconductors by the inverse proximity effect [23] and hence Ising superconductors can be created from the usual superconducting thin films.

Technically, achieving good metal contact to the monolayer WSe_2 has always been challenging, although different contact methods have been tried [24,25]. For example, graphene has been used as a terminal in the transport measurements of MoS_2-based heterostructures and quantum oscillations have been observed in the whole system [24]. In our study, the contact issue of monolayer WSe_2 is excluded since we focus on the superconducting behavior of metallic thin films which are coupled to monolayer WSe_2. On the other side, the proximity effect between 2D materials is very pronounced. For example, strong SOI has been successfully induced into graphene/WS_2 and, as a result, a weak antilocalization effect at low temperatures and small spin-relaxation time have been obtained in graphene [26].

In this Rapid Communication, we demonstrate that strong SOI can be induced into Al thin films (with a coherence length $\sim$1600 nm [27,28]) by coupling to monolayer WSe_2, which protects the Cooper pairs from the in-plane magnetic field and enhances the upper critical field. This was manifested in transport and magnetotransport measurements of Al with different thicknesses on WSe_2 (the results for Nb [29] samples are also obtained and shown in the Supplemental Material [30]). Superconducting behaviors of Al thin films with a thickness from 7 to 10 nm are studied using transport measurements. The proximity effect between the TMDs with strong SOI and a conventional superconductor enlarges the B–T superconducting phase diagram significantly. Theoretically, we consider both the Zeeman effect and the orbital effect of the field, and show that strong SOI is induced into superconducting Al thin films from monolayer WSe_2.

The band structure of monolayer WSe_2 is calculated from the first principles including SOI and is shown in Fig. 1(a). It has a direct band gap of $\sim$1.26 eV at the K point. The valence band is split due to Ising SOI, which is largest ($\sim$500 meV) at the K point. The schematic view and microscopy image of the device are shown in Fig. 1(b). After the exfoliation of monolayer WSe_2 onto the substrate, the Al is evaporated on top with the patterns defined by electron-beam lithography. Then we adopt the photoluminescence (PL) and Raman spectroscopy measurement to characterize the monolayer WSe_2 as

*These authors contributed equally to this work.
†Corresponding author: phwang@ust.hk

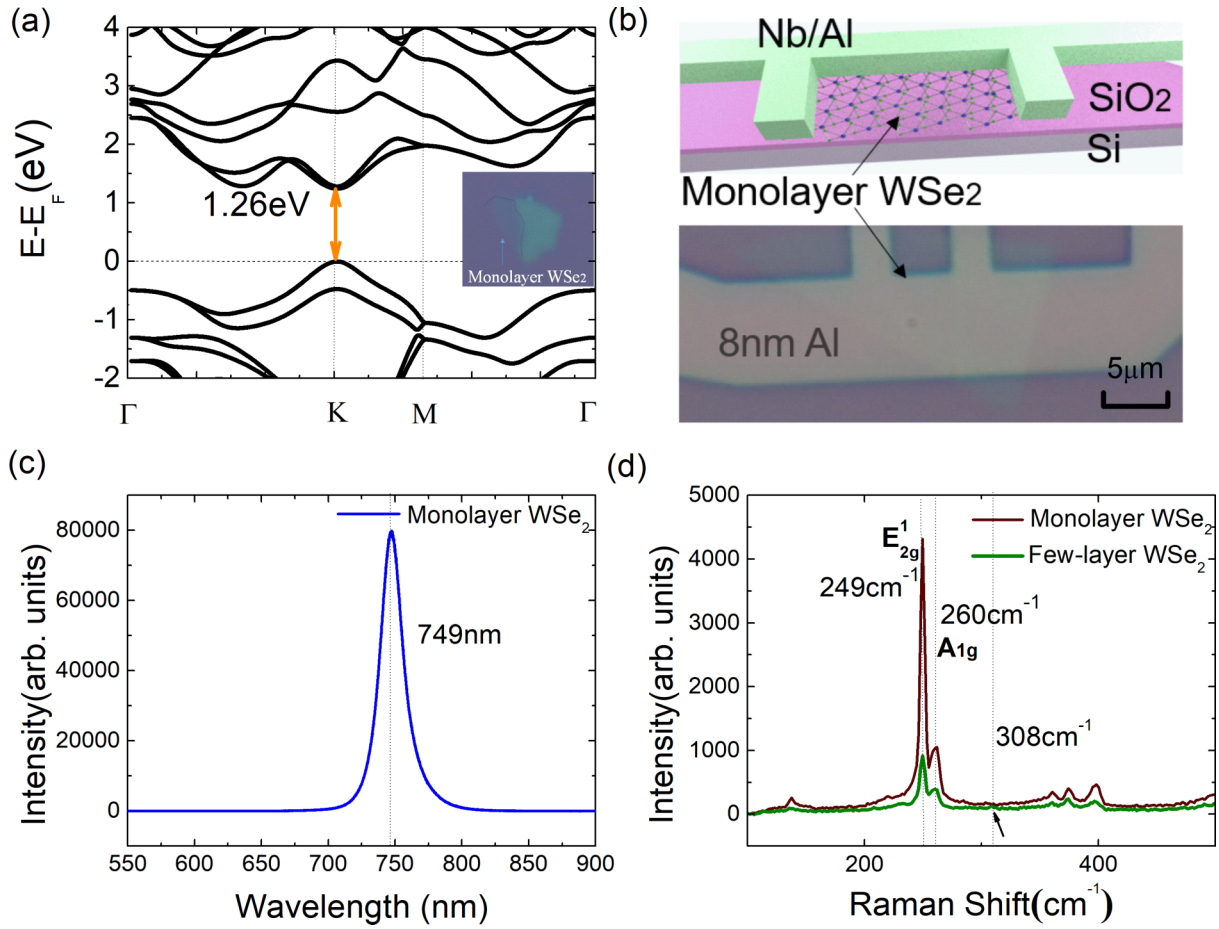

FIG.1. Characteristics of monolayer WSe_2 and Al/WSe_2 heterostructure. (a) The direct band gap for monolayer WSe_2 at the K point. The inset shows the microscopy image of monolayer WSe_2. (b) Schematic and microscopy images of Al thin films on top of monolayer WSe_2 which is supported on a 300 nm SiO_2/Si substrate. (c) The photoluminescence and (d) Raman spectroscopy measurements for monolayer WSe_2 and few-layer WSe_2. The arrow indicates the peak at 308 cm^{-1} for few-layer WSe_2.

shown in Figs. 1(c) and 1(d). PL demonstrates a direct band gap of ∼1.6 eV. This agrees with other optical measurements [31,32] and is larger than that of our first-principles calculation. The underestimation of the gap in the calculation is due to the approximation in the calculation method [33]. Two typical Raman oscillation modes have been observed at 249 and 260 cm^{-1}, which correspond to the E^1_{2g} and A_{1g} modes, respectively [34,35]. The E^1_{2g} mode results from the in-plane vibration, while A_{1g} is related to the vibration of selenium atoms along the out-of-plane direction. For few-layer WSe_2, a peak around the Raman shift of 308 cm^{-1} will be induced due to the van der Waals force between two adjacent layers. The absence of this peak is an evidence for monolayer WSe_2.

After assembly of this superconductor/TMD heterostructure, we measure the magnetoresistance with the lock-in technique. We carry out the transport measurements both on the Al/WSe_2 and Nb/WSe_2 heterostructures and, in both systems, Ising SOI has been induced into the metallic thin films. The data for the Al/WSe_2 bilayer are obtained using a helium-3 probe, which can cool the sample temperatures down to 300 mK, and measured with four probes. We present the data of pristine Al thin films first. When we apply the in-plane magnetic field to Al thin films, superconductivity is gradually suppressed when the magnetic field is increased, as shown in Fig. 2(a). The critical temperature at a specific magnetic field is defined as the temperature corresponding to $0.5R_0$ and R_0 is the resistance at 2 K (before superconductivity happens). After extracting the critical temperatures at different magnetic fields, we can get the B–T superconducting phase diagrams of Al thin films with a varied thickness of 10, 8, and 7 nm separately, as shown in Fig. 2(b). The 10-nm-thick Al thin films show a linear relation in the phase diagram which is similar to that of a bulk sample, while the 8-nm-thick Al thin films already deviated from a linear relation and shows a 2D behavior.

The zero-field critical temperature of Al increases when the Al thickness is reduced, as shown in the inset of Fig. 2(b). In the framework of BCS superconductivity theory without making use of any new electron-pairing mechanism, the theory of Shapoval [36] suggests that in the case of $\Delta T \ll T_{c\infty}$, the change in critical temperature ΔT follows the following relation due to size limitations:

$$\frac{\Delta T}{T_{c\infty}} = \frac{\alpha S}{2p_\infty V}\ln\frac{2\xi\omega_D}{\pi T_{c\infty}}. \quad (1)$$

Here, $T_{c\infty}$ is the critical temperature with infinite volume (for the bulk in this case). $\alpha \approx \pi/4$ and $\xi \approx 1.78$ for thin films. d is the thickness, p_∞ is the Fermi momentum at an

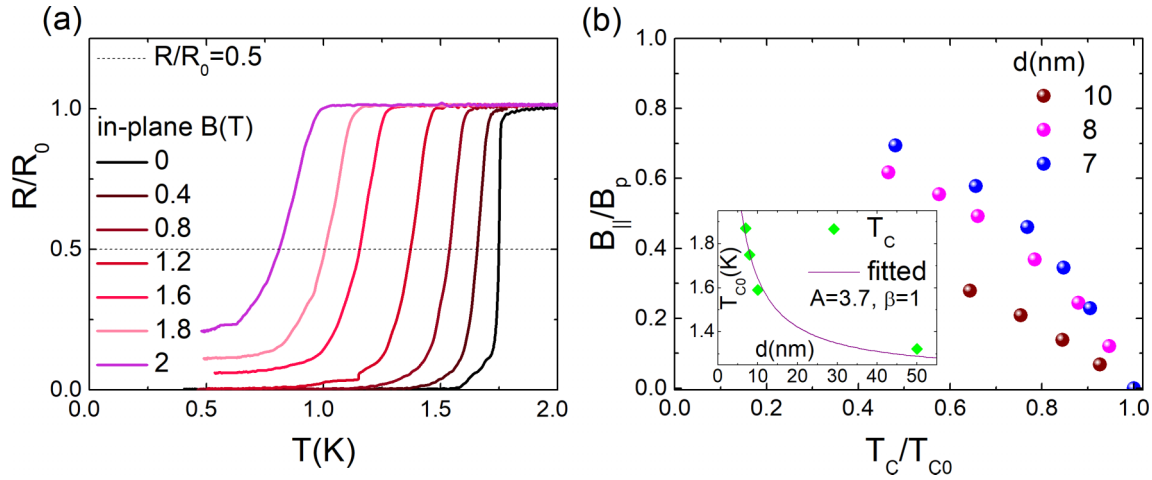

FIG. 2. Pauli limit for Al superconducting thin films, a conventional type-I superconductor. (a) Destroyed Cooper pairs by the in-plane magnetic fields for 8-nm-thick Al thin film. (b) B–T superconducting phase diagram for Al thin films. The inset shows the increasing superconducting temperatures for the decreased Al thicknesses.

infinite volume, and ω_D is the Debye frequency. S and V are the surface area and volume, respectively. For thin films $\sim$10 nm, a rise of critical temperature is expected to be by 10−15%. However, our data show a 50% increase of T_C compared to that of the bulk. This discrepancy results from the errors of $\frac{S}{V}$, which is probably not $\frac{2}{d}$ (this value is for a parallel plate model) due to the existence of the interface surface area from the polycrystalline properties of our evaporated Al thin films [37]. Besides, this theory indicates that a change of the temperature shows the following dependence: $\Delta T/T_{c\infty} = A/d^{\beta}$. The fitting curve is shown in the inset of Fig. 2(b), where we get the parameters $A = 3.7$ and $\beta = 1$ when $T_{c\infty} =$ 1.2 K. This fitting result is consistent with Eq. (1).

With monolayer or multilayer WSe_2 coupled to Al thin films, the superconducting behavior of Al has been significantly modified. Figure 3(a) shows the effect of the magnetic field on the superconductivity for an 8-nm-thick Al/monolayer WSe_2 heterostructure. At a magnetic field of 2 T and a temperature of 0.5 K, the superconductivity is more robust in the Al/WSe_2 heterostructure compared to Fig. 2 where, in pristine 8-nm-thick Al, the superconductivity is partially destroyed.

We note that WSe_2 underneath can slightly lower the critical temperature of Al (more information can be found in Fig. S1 in the Supplemental Material [30]), which is not surprising considering leakage of the Cooper pairs. The change is small here because WSe_2 is gapped. It turned out that the influence of WSe_2 on the T_C decreases as the thickness of the metallic thin film increases, as shown in the inset of Fig. 3(b), or as the thickness of WSe_2 increases (as shown in the Supplemental Material [30]). For example, the superconducting critical temperatures at a zero-field T_{C0} for 7-nm-thick Al, 7-nm-thick Al/monolayer WSe_2, and 7-nm-thick Al/few-layer WSe_2 samples are 1.87, 1.81, and 1.83 K, respectively. These may be explained through the change of the band structure from monolayer to bulk WSe_2. First-principles calculations show that the electron states nearest the Fermi level shift from K pocket to Γ pocket as the thickness increases. As one direction (say the z direction) of the Al/Nb becomes short,

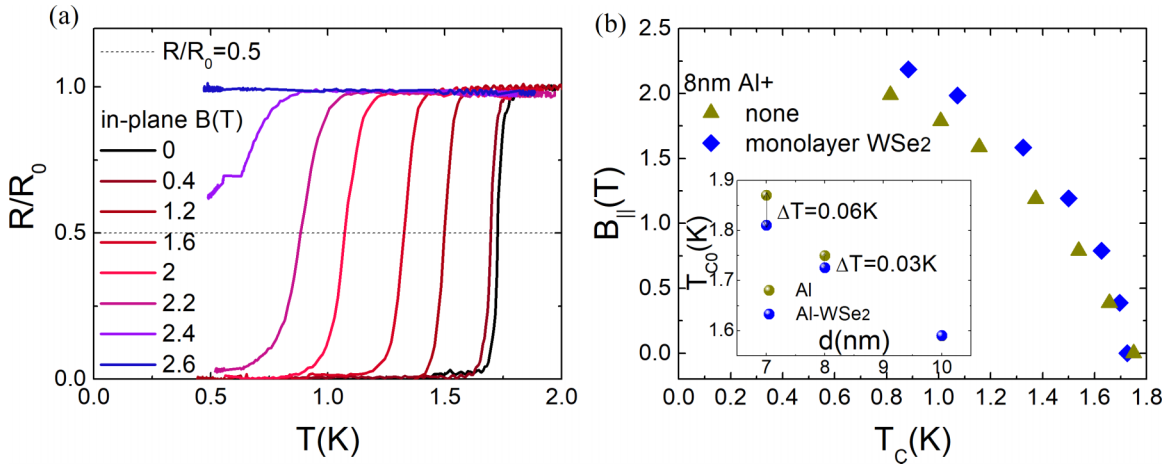

FIG. 3. Proximity effects on the critical temperatures in 8-nm-thick Al/ monolayer WSe_2 heterostructure. (a) Resistance dependence on the temperature at different applied magnetic fields and (b) extracted critical temperatures at different in-plane magnetic fields. The inset shows the difference in zero-field critical temperatures between Al and Al/WSe_2 samples for various thickness of Al.

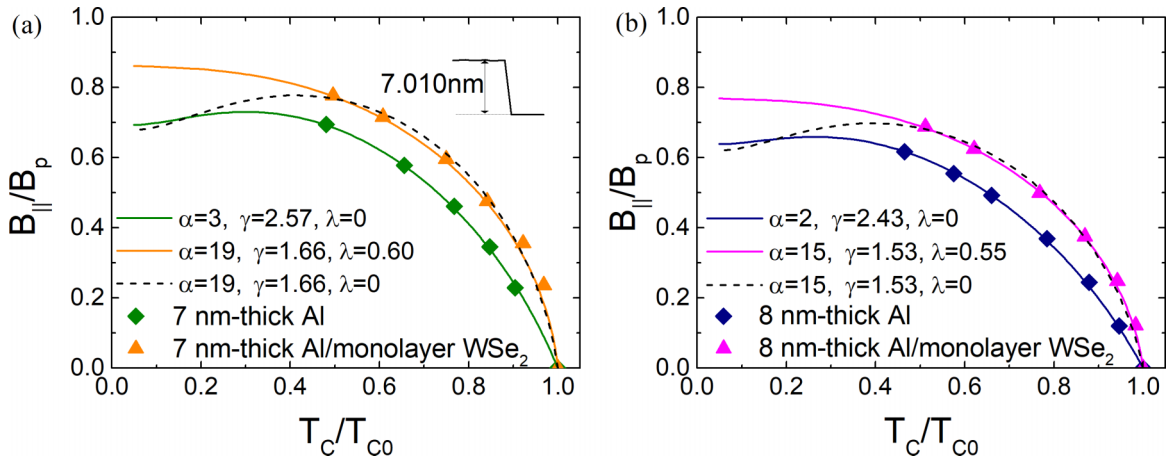

FIG. 4. Phase diagram for Al and Al/WSe_2 samples. Normalized phase diagram for (a) 7-nm-thick (inset shows the thickness obtained from atomic force measurements) and (b) 8-nm-thick Al and Al on monolayer WSe_2. The dots are experimental data and the lines are fitting curves based on Eq. (2). The corresponding parameters are listed.

the quantization of the wave vector k_z becomes significant and the density of state on the Fermi surface is larger near $\sqrt{k_x^2+k_y^2} \sim k_F$ than that near the Γ point where $\sqrt{k_x^2+k_y^2} \sim 0$ (k_F is the Fermi wave vector). As a result, the coupling between WSe_2 and Al thinner films is stronger near the K pocket, which is closer to k_F, than near the Γ pocket.

After extraction of the critical temperatures, we obtain the phase diagram as shown in Fig. 3(b), and Fig. 4 shows the normalized phase diagrams. The magnetic field is normalized by the Clogston-Chandrasekhar Pauli limit, which is determined by $\sqrt{2}\mu_B B_p = 1.76 k_B T_{C0}$, i.e., $B_p = 1.84 T_{C0}$. For the pristine Al thin film, the curve is linear near T_{C0}, but the critical field exceeds that of bulk samples (0.2 T in-plane field for a 50-nm-thick Al film). This shows that both the orbital effect and Zeeman effect of the magnetic field are important in suppressing the superconductivity. Furthermore, we expect our sample to be in the regime of dirty superconductors because of the inevitable impurities induced from the fabrication process. In this case, the relation between the magnetic fields $B_{||}$ and the critical temperature T_C is described by the following equation [38]:

$$\ln\frac{1}{t} = \sum_{n=-\infty}^{+\infty}\left[\frac{1}{|2n+1|} - \left(|2n+1| + \frac{B_{||}}{\gamma t \alpha B_p} + \frac{\frac{B_{||}^2}{\gamma^2 t^2 B_p^2}}{|2n+1| + \frac{B_{||}}{\gamma t \alpha B_p} + \frac{\lambda}{t}}\right)^{-1}\right], \tag{2}$$

where $t = T_C/T_{C0}$ is the normalized critical temperature. The three dimensionless parameters are defined as $\alpha = 3\hbar/2mv_F^2\tau$, $\gamma = 1.6\pi m\mu_B/\hbar e = 0.8\pi m/m_e$, and $\lambda = \hbar/3\pi\tau_{SO}k_B T_{C0}$, where m, v_F, and τ are the effective electron mass, the Fermi velocity, and the scattering time, respectively. The constants μ_B, k_B, m_e, and e are the Bohr magneton, the Boltzmann constant, the free electron mass, and the magnitude of electron charge, respectively. τ_{SO} is the spin-orbit scattering time. Dirty samples correspond to $\tau k_B T_{C0} \ll \hbar$.

The fitting curves for both the 7-nm-thick and 8-nm-thick Al samples based on Eq. (2) are shown in Fig. 4 as well as the corresponding parameters. For both thicknesses, the case without WSe_2 can be fit very well by tuning only two parameters α and γ, while the spin-orbit scattering is totally excluded, i.e., $\lambda = 0$. However, for the case with the monolayer WSe_2, the data cannot fit with $\lambda = 0$ as indicated by the dashed fitting curves. Instead, we found for the 8 nm case that the best fitting yields $\lambda = 0.554$, which corresponds to a spin-orbit scattering time of $\tau_{SO} = 0.8$ ps. This provides as direct evidence that SOI is induced in the Al thin films by proximity of the monolayer WSe_2. In our measurement, the critical field is not enhanced as much as that in intrinsic Ising superconductors (say $NbSe_2$ and gated MoS_2). On one hand, the effective SOI induced by the proximity effect is much weaker than that of intrinsic Ising superconductors due to the weak coupling between the Al films and the WSe_2, the mismatch between their Fermi surfaces, possible Rashba spin-orbit coupling induced at the interface, disorder, etc. On the other hand, the orbital effect still plays a role here, which is clear from the linear behavior of the critical field near T_{C0} without WSe_2. The 7-nm-thick Al sample has a larger λ and thus a stronger SOI induced by WSe_2. This is just as expected since λ is proportional to an averaged value of the induced SOI, which should have maximum value at the interface and decays as the distance from the interface increases. Consequently, the thicker Al sample has a smaller averaged SOI.

According to the fitting parameters, the effective mass of the 8-nm-thick Al samples can be estimated to be $1.0m_e$ without WSe_2 and $0.6m_e$ with WSe_2. The decrease of the

effective mass can be attributed to the leakage of electrons into the WSe_2 layer [39], which has a smaller effective mass of $0.45m_e$ [40]. The total effective electron mass is, in some sense, averaged, as the case of quantum well in Ref. [39]. For 7-nm-thick samples, we obtained larger effective masses both with and without WSe_2. This is consistent with the thickness dependence of the effective mass in quantum wells [39,41]. Unlike the effective mass, v_F cannot be deduced directly from the fitting parameters. However, due to the weak coupling between Al and WSe_2 (which should be van der Waals coupling considering the layered structure of WSe_2), it is reasonable to assume that the change in Fermi energy is relatively small, i.e., mv_F^2 is almost unchanged. Then, according to the values of the fitting parameter α, the scattering time τ in the Al/WSe_2 sample is reduced to about 1/6 of that in the pristine Al samples (for both thicknesses of 7 and 8 nm). This is in qualitative agreement with the normal resistance measurement above T_C (for example, 0.7 $k\Omega$ without WSe_2 and 3 $k\Omega$ with WSe_2 for 8-nm-thick samples at 2 K) and it is attributed to a greater roughness induced by coupling to WSe_2 [39]. It is also interesting to note that the fitting parameter α is larger in thinner samples. This indicates that the thinner Al film has a smaller scattering time and thus a stronger disorder as expected because thinner samples should be more sensitive to the fabrication environment. For instance, the rough interface between the Al films and the oxidized Al_2O_3 layer is likely to have a stronger effect in thinner films.

In summary, we have systematically studied superconducting Al thin films in proximity to semiconducting monolayer and few-layer WSe_2 (see Supplemental Material [30]). We find that the critical temperature increases as the thickness of the Al thin films decreases. The superconducting critical temperature for a heterostructure of 8-nm-thick Al and monolayer WSe_2 is slightly decreased compared to that of pristine 8-nm-thick Al. When the WSe_2 is thick enough, the critical temperature of Al films is almost unchanged, as shown in Fig. S1 of the Supplemental Material [30]. Promisingly, the in-plane critical field of Al thin films is enhanced about 10% by coupling to WSe_2. Combining our data with theory, we conclude that spin-orbit scattering, and thus spin-orbit interaction, is induced in the superconducting films by the proximity of WSe_2. Furthermore, there are many TMDs with extremely large SOI. Our results demonstrate a feasible approach to combine these strong SOI in TMDs with conventional thin-film superconductors. With improved quality of thin-film superconductors and optimized coupling at the superconductor/TMD interface, proximity-induced Ising superconductivity with larger in-plane critical field enhancement could be expected in a heterostructure of monolayer TMD and thin-film superconductor at a 2D limit. This large in-plane field could drive the heterostructure into a nodal topological phase [23,42], which could be used to realize Majorana fermions at higher temperatures and have applications in superconducting spintronics.

The authors are grateful for financial support from the Research Grants Council of Hong Kong (Projects No. 16300717 and No. C7036-17W) and technical support of the Raith-HKUST Nanotechnology Laboratory for the electron-beam lithography facility and electron microscopy facility at MCPF (Project No. C6021-14E).

[1] L. Li, G. J. Ye, V. Tran, R. Fei, G. Chen, H. Wang, J. Wang, K. Watanabe, T. Taniguchi, L. Yang, X. H. Chen, and Y. Zhang, Nat. Nanotechnol. **10**, 608 (2015).
[2] F. Xia, H. Wang, and Y. Jia, Nat. Commun. **5**, 4458 (2014).
[3] V. Tran, R. Soklaski, Y. Liang, and L. Yang, Phys. Rev. B **89**, 235319 (2014).
[4] M. Buscema, D. J. Groenendijk, S. I. Blanter, G. A. Steele, H. S. J. Van Der Zant, and A. Castellanos-Gomez, Nano Lett. **14**, 3347 (2014).
[5] Y. Wu, X. Chen, Z. Wu, S. Xu, T. Han, J. Lin, B. Skinner, Y. Cai, Y. He, C. Cheng, and N. Wang, Phys. Rev. B **93**, 035455 (2016).
[6] J. M. Lu, O. Zeliuk, I. Leermakers, N. F. Q. Yuan, U. Zeitler, K. T. Law, and J. T. Ye, Science **350**, 1353 (2015) .
[7] A. Srivastava, M. Sidler, A. V. Allain, D. S. Lembke, A. Kis, and A. Imamoglu, Nat. Phys. **11**, 141 (2015).
[8] H. J. Chuang, X. Tan, N. J. Ghimire, M. M. Perera, B. Chamlagain, M. M.-C. Cheng, J. Yan, D. Mandrus, D. Tománek, and Z. Zhou, Nano Lett. **14**, 3594 (2014).
[9] G. Aivazian, Z. Gong, A. M. Jones, R. L. Chu, J. Yan, D. G. Mandrus, C. Zhang, D. Cobden, W. Yao, and X. Xu, Nat. Phys. **11**, 148 (2015).
[10] H. Zeng, J. Dai, W. Yao, D. Xiao, and X. Cui, Nat. Nanotechnol. **7**, 490 (2012).
[11] O. Lopez-Sanchez, D. Lembke, M. Kayci, A. Radenovic, and A. Kis, Nat. Nanotechnol. **8**, 497 (2013).
[12] A. K. Geim and K. S. Novoselov, Nat. Mater. **6**, 183 (2007).
[13] B. Radisavljevic, A. Radenovic, J. Brivio, V. Giacometti, and A. Kis, Nat. Nanotechnol. **6**, 147 (2011).
[14] A. Splendiani, L. Sun, Y. Zhang, T. Li, J. Kim, C.-Y. Chim, G. Galli, and F. Wang, Nano Lett. **10**, 1271 (2010).
[15] Q. H. Wang, K. Kalantar-Zadeh, A. Kis, J. N. Coleman, and M. S. Strano, Nat. Nanotechnol. **7**, 699 (2012).
[16] X. Xu, W. Yao, D. Xiao, and T. F. Heinz, Nat. Phys. **10**, 343 (2014).
[17] K. Kosmider, J. W. González, and J. Fernández-Rossier, Phys. Rev. B **88**, 245436 (2013).
[18] Z. Y. Zhu, Y. C. Cheng, and U. Schwingenschlögl, Phys. Rev. B **84**, 153402 (2011).
[19] A. Kormányos, V. Zólyomi, N. D. Drummond, and G. Burkard, Phys. Rev. X **4**, 039901 (2014).
[20] X. Xi, Z. Wang, W. Zhao, J.-H. Park, K. T. Law, H. Berger, L. Forró, J. Shan, and K. F. Mak, Nat. Phys. **12**, 139 (2016).
[21] B. S. Chandrasekhar, Appl. Phys. Lett. **1**, 7 (1962).
[22] P. M. Tedrow and R. Meservey, Phys. Rev. B **25**, 171 (1982).
[23] R. Wakatsuki and K. T. Law, arXiv:1604.04898, 2016.
[24] X. Cui, G. H. Lee, Y. D. Kim, G. Arefe, P. Y. Huang, C. H. Lee, D. A. Chenet, X. Zhang, L. Wang, F. Ye, F. Pizzocchero,

B. S. Jessen, K. Watanabe, T. Taniguchi, D. A. Muller, T. Low, P. Kim, and J. Hone, Nat. Nanotechnol. **10**, 534 (2015).
[25] H. C. P. Movva, A. Rai, S. Kang, K. Kim, B. Fallahazad, T. Taniguchi, K. Watanabe, E. Tutuc, and S. K. Banerjee, ACS Nano **9**, 10402 (2015).
[26] Z. Wang, D. K. Ki, H. Chen, H. Berger, A. H. MacDonald, and A. F. Morpurgo, Nat. Commun. **6**, 8339 (2015).
[27] M. D. Maloney, F. de la Cruz, and M. Cardona, Phys. Rev. B **5**, 3558 (1972).
[28] R. W. Cohen and B. ABeles, Phys. Rev. **168**, 444 (1968).
[29] R. F. Gasparovic and W. L. McLean, Phys. Rev. B **2**, 2519 (1970).
[30] See Supplemental Material at http://link.aps.org/supplemental/10.1103/PhysRevB.99.121406 for the proximity effect between WSe_2 and Nb thin films, WSe_2 underneath which can slightly lower the critical temperature of Al, the influence of WSe_2 thickness on the critical temperature, and coupling Al thin films to few-layer WSe_2.
[31] H. Zeng, G.-B. Liu, J. Dai, Y. Yan, B. Zhu, R. He, L. Xie, S. Q Xu, X. Chen, W. Yao, and X. Cui, Sci. Rep. **3**, 1608 (2013).
[32] W. Zhao, R. M. Ribeiro, M. Toh, A. Carvalho, C. Kloc, A. H. Castro Neto, and G. Eda, Nano Lett. **13**, 5627 (2013).
[33] W. Huang, X. Luo, C. K. Gan, S. Y. Quek, and G. Liang, Phys. Chem. Chem. Phys. **16**, 10866 (2014).
[34] P. Tonndorf, R. Schmidt, P. Böttger, X. Zhang, J. Börner, A. Liebig, M. Albrecht, C. Kloc, O. Gordan, D. R. T. Zahn, S. M. de Vasconcellos, and R. Bratschitsch, Opt. Express **21**, 4908 (2013).
[35] E. Del Corro, H. Terrones, A. Elias, C. Fantini, S. Feng, M. A. Nguyen, T. E. Mallouk, M. Terrones, and M. A. Pimenta, ACS Nano **8**, 9629 (2014).
[36] E. A. Shapoval, ZhETF Pisma Redaktsiiu **5**, 57 (1967).
[37] P. N. Chubov, V. V Eremenko, and Y. A. Pilipenko, Zh. Eksp. Teor. Fiz **28**, 752 (1969).
[38] N. R. Werthamer, E. Helfand, and P. C. Hohenberg, Phys. Rev. **147**, 295 (1966).
[39] C. Wetzel, A. L. Efros, A. Moll, B. K. Meyer, P. Omling, and P. Sobkowicz, Phys. Rev. B **45**, 14052 (1992).
[40] B. Fallahazad, H. C. P. Movva, K. Kim, S. Larentis, T. Taniguchi, K. Watanabe, S. K. Banerjee, and E. Tutuc, Phys. Rev. Lett. **116**, 086601 (2016).
[41] U. Ekenberg, Phys. Rev. B **40**, 7714 (1989).
[42] B. T. Zhou, N. F. Q. Yuan, H. L. Jiang, and K. T. Law, Phys. Rev. B **93**, 180501 (2016).